Capturing directed molecular motion in the nuclear pore complex of live cells

Francesco Cardarelli[a], Luca Lanzano[b], and Enrico Gratton[b,1]

[a]Center for Nanotechnology Innovation at National Enterprise for nanoScience and nanoTechnology, Istituto Italiano di Tecnologia, 56127 Pisa, Italy; and [b]Laboratory for Fluorescence Dynamics, Department of Biomedical Engineering, University of California, Irvine, CA 92697

Edited by* Jennifer Lippincott-Schwartz, National Institutes of Health, Bethesda, MD, and approved May 9, 2012 (received for review January 10, 2012)

Nuclear pore complexes (NPCs) are gateways for nucleocytoplasmic exchange. Intrinsically disordered nucleoporins (Nups) form a selective filter inside the NPC, taking a central role in the vital nucleocytoplasmic transport mechanism. How such intricate meshwork relates to function and gives rise to a transport mechanism is still unclear. Here we set out to tackle this issue in intact cells by an established combination of fluorescence correlation spectroscopy and real-time tracking of the center of mass of single NPCs. We find the dynamics of nucleoporin Nup153 to be regulated so as to produce rapid, discrete exchange between two separate positions within the NPC. A similar behavior is also observed for both karyopherinβ1 transport-receptor and cargoes destined to nuclear import. Thus, we argue that directed Nup-mediated molecular motion may represent an intrinsic feature of the overall selective gating through intact NPCs.

fluctuation spectroscopy | particle tracking

Nuclear pore complexes (NPCs) regulate the exchange of macromolecules between the nucleus and the cytoplasm (1, 2). Each eukaryotic NPC is an approximately 120-MDa supramolecular complex of about 30 different polypeptides designated nucleoporins (Nups) (3) approximately one-third of which are rich in natively unfolded Phe-Gly (FG) repeat domains (4). They form a selective filter inside the NPC that inhibits the efficient translocation of large cargo molecules (>40 kD) (5), unless they are chaperoned by transport receptors known as karyopherins (Kaps; also called importins and exportins) (6). In spite of the progress made in understanding NPC structure and its implications for nucleocytoplasmic transport, several aspects of how individual NPCs facilitate cargo translocation remain unresolved and represent a formidable challenge in present research. Such uncertainties stem from the complex nature of NPCs and from limitations associated with the current experimental approaches used to probe the NPC mechanism at the nanomolecular level and under real-time trafficking conditions. One of the controversies surrounding the field involves the origin of the "paradoxical" selective gating mechanism, which remains largely unknown. Different figurative translocation models have been proposed so far (for a review see ref. 2). In the "virtual gating" model (7), the NPC allocates a large channel decorated at both the cytoplasmic and nucleoplasmic entrances with several FG-Nup fibrils. In this scheme, flexible and largely unstructured FG-domains limit available space in the NPC near field, thus restricting access of nontransport substrates to the channel. Conversely, FG-Nups increase the residence time of transport complexes in the central aperture of the pore by binding to nuclear transport receptors. In this way, FG-Nups facilitate diffusion of transport complexes into the central channel. In the "affinity gradient" model (8), FG-Nups are arranged along the NPC channel that their affinity for FG-binding molecules increases along the NPC axis. FG-binding molecules would permeate the NPC by being handed over from one nucleoporin with lower affinity to the neighboring one with higher affinity. In the "reduction of dimensionality" model the filaments and the central channel of the NPC are lined by a coherent FG surface, while a selectivity filter restricts the passage of neutral molecules to a narrow tube in the channel center (9): Here transport complexes first bind to filaments at the channel entrance and then slide on the FG surface by a two-dimensional search for the channel exit. In contrast, the "selective phase" model describes Kap movement across the pore as a "permeation/melting through a gel-like selective phase" (5). In fact, the authors demonstrated that yeast FG-Nups can form a supramolecular hydrogel in vitro, with properties reminiscent of the physiological NPC permeability barrier (10–12). This gel-like behavior of the NPC is directly contrasted by the nanoscale mechanochemical properties of selected FG-Nups measured in vitro (13, 14). In this case, in fact, the FG repeats of nucleoporin Nup153 are proved to form a noncohesive brush in vitro, which is able to be reversibly collapsed by interactions with the Karyopherinβ1 (Kapβ1) receptor. The emerging complex picture of NPC structure and function is somewhat taken into account within the "hybrid" model recently proposed by Yamada et al. (15). The authors found that the yeast FG domains are structurally and chemically heterogeneous, adopting either globular, collapsed coil configurations and more dynamic, extended coil conformations. In addition, several FG-Nups can feature both types of structures in a bimodal distribution along the polypeptide chain. Notably, these features are not randomly distributed, as they are assumed to form a tubular gate structure or transporter at the NPC center featuring two separate zones of traffic with distinct physicochemical properties.

In our opinion, an intriguing part of such ambiguities fall beyond the overall structural aspects of an NPC and instead pertain to how individual components of the pore (e.g., FG-Nups) affect/regulate nucleocytoplasmic transport. In general, within the proposed models, diffusion and directed motion are opposed as the two candidate mechanisms responsible for propelling the cargo (and receptor) molecules through the pore. Diffusion and directed motion, however, have different spatiotemporal behaviors and we should be able to separate these two possibilities with properly designed experiments. To this end, we recently set up a microscope that combines fluorescence correlation spectroscopy (FCS) with real-time orbital tracking of single pores in live cells (16). From the privileged observation point located in the reference system of the NPC we can study the pore behavior with high temporal and spatial resolution. It is clear that the elucidation of complex nanoscale effects, such as those described above, necessitate the need to probe and understand the behavior of individual components of the NPC. As a first relevant molecule we analyze a C-terminally GFP-tagged version of Nup153. Nup153 is a well-studied FG-nucleoporin, which is known to be critical for both nuclear import and nuclear export (for a review see ref. 17).

Author contributions: F.C. and E.G. designed research; F.C. and L.L. performed research; F.C. and L.L. analyzed data; and F.C. and E.G. wrote the paper.

The authors declare no conflict of interest.

*This Direct Submission article had a prearranged editor.

Freely available online through the PNAS open access option.

[1]To whom correspondence should be addressed. E-mail: egratton22@yahoo.com.

This article contains supporting information online at www.pnas.org/lookup/suppl/doi:10.1073/pnas.1200486109/-/DCSupplemental.

Nup153 is anchored to the nuclear basket of the NPC through its N-terminal domain (18). At the same time it is hypothesized that the long, mobile FG-rich C-terminal domain of Nup153 is able to bind cargo located anywhere within its reach, even close to the cytoplasmic side of the pore (18). By rapidly orbiting around the center of mass of Nup153-GFP distribution, we detect a previously hidden dynamic behavior regulated so as to produce rapid, discrete exchange of the GFP tag between two separate positions within the NPC. Next, we show that this highly regulated vectorial exchange is shared by the Kapβ1 receptor during transport. Finally, by cross-correlation of the two signals, we show that Nup153 activity is compatible with the functional nuclear import of a classical NLS-bearing cargo. Based on these evidences, we propose that Nup-mediated directed motion may contribute to the selective gating of molecules through intact NPCs. We do believe our results pave the way for future investigations of NPC function in intact cells.

Results and Discussion

Analysis of Single Nup153-GFP Dynamics Within the NPC. To investigate the barrier-like behavior of the FG domains during transport, we use a C-terminally GFP-labeled adduct of nucleoporin Nup153 transiently transfected into live CHO-K1 cells (Fig. 1*A*). It has been demonstrated by others that GFP-variants of Nup153 are correctly targeted and incorporated into NPCs (19–21). In addition, it was shown that Nup153-GFP dynamically interacts with the pore, with two characteristic residence times in the range of minutes (19, 20). This overall slow turnover defines the lifetime of Nup153 association with the NPC and is well separated from the characteristic timescale (millisecond range) of nucleocytoplasmic transport we want to address here. During transport, as schematically shown in Fig. 1*B*, the flexible FG-repeat carboxy-terminal domain (here tagged to GFP) extends towards the central channel where it is supposed to interact with soluble transport receptors [i.e., Kapβ1, (14)] and promote their translocation to the nucleus (18). A schematic representation of

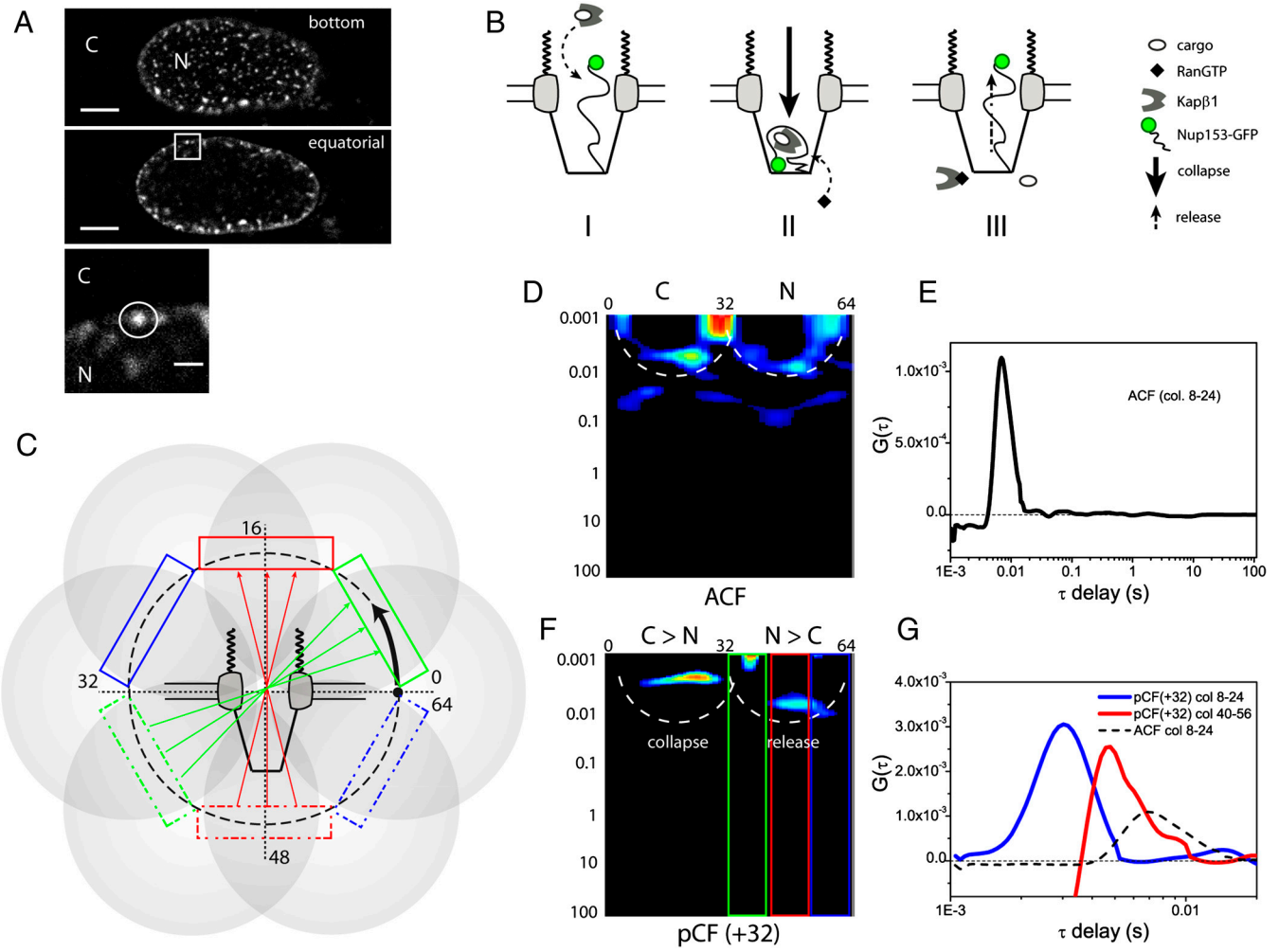

Fig. 1. (*A*) Cell expressing Nup153-GFP (scale bar: 5 μm) imaged at different *z* positions. Nup153-GFP accumulation on single pores is better shown in the *Bottom* (scale bar: 1 μm). (*B*) Schematic representation of the accepted model of Nup153 activity: It binds to the Kap-cargo complex on the cytoplasmic face of the NPC (I), collapses towards the nucleus (II), and is finally released by RanGTP (III). (*C*) The PSF is scanned along a 64-points orbit (R = 120 nm) around the pore, as described in the text. (*D*) The ACF is displayed in a pseudo-color carpet in which the *x* coordinate corresponds to the points along the orbit and the *y* coordinate to the autocorrelation time (log-scale). (*E*) The average ACF of columns 8–24 quantitatively describes the hump of the cytoplasmic arc. (*F*) The pair correlation function at the distance of 32 pixels along the orbit [pCF(+32)] identifies two characteristic times of Nup153 molecular movement at the pore: a fast cytoplasm-to-nucleus collapse (peak position: 3.1 ms; FWHM: 1.8) and a slower nucleus-to-cytoplasm release (region highlighted by the red square in the pCF carpet and in *C*; correlation peak position: 5 ms; FWHM: 2.4). By contrast, almost no correlation is detected at the same distance but quite perpendicular to the channel (regions highlighted by the green and blue squares in the pCF carpet and in *C*). (*G*) The collapse/release components are here compared to the total ACF (dashed line).

Table 1. Cumulative results from fluorescence correlation analysis along the orbit

	ACF		pCF(C > N)		pCF(N > C)		
	Peak position	FWHM	Peak position	FWHM	Peak position	FWHM	N
Nup153-GFP	7.5 ± 2.2	5.0 ± 1.8	3.0 ± 0.7	1.4 ± 0.6	5.1 ± 0.9	1.7 ± 0.6	25
NLS-mCherry	—	—	3.5 ± 1.0 (27 ± 18)	2.0 ± 0.7 (92 ± 48)	28 ± 15	88 ± 38	5
Kapβ1-GFP*	*9.6 ± 3.5*	*13 ± 6.5*	*3.3 ± 1.8*	*1.2 ± 0.3*	*3.2 ± 1.5*	*1.3 ± 0.3*	25
mCherry	—	—	35 ± 18	120 ± 54	31 ± 17	111 ± 41	6

Peak position and FWHM for all the analyzed cells (N). Numbers are expressed in milliseconds (mean SD). The pCF is calculated always at the distance of 32 pixels along the orbit.
*Kapβ1-GFP values taken from our previous analysis (16).

the experiment is shown in Fig. 1*C*: A circular light envelope is formed around the pore by a scanning laser spot [point spread function (PSF)] around the pore in 0.5–1 ms, while the real-time tracking routine keeps the center of mass of the NPC always at the center of the orbit* (see *Materials and Methods*). The scan start point is known (Fig. S1) and positioned along the nuclear envelope plane (black dot in Fig. 1*C*), with the first half of the orbit scanning through the cytoplasmic face of the NPC. The orbit radius is usually set to approximately 120 nm, which we found to be optimal for the accuracy of tracking (see *Materials and Methods*). The intensity along the orbit is measured at 64 points in the NPC reference system and fluctuation analysis is performed to extract information on single Nup153-GFP molecules dynamics within the pore. The autocorrelation function (ACF) carpet unequivocally shows a spatiotemporal regulation of Nup153-GFP dynamics, which produces a peculiar "double-arc" shape of the correlation profile (Fig. 1*D*). As shown in the plot of Fig. 1*E*, the hump of the arc (e.g., columns 8–24) depicts a narrow distribution of correlation times in the ACF. Notably, these features are reminiscent of what we observed in the ACF analysis of Kapβ1 shuttling (16). Thus we are prompted to interpret the hump as a characteristic time of Nup153-GFP movement at the pore, with the same GFP being detected in one position along the orbit at time t and again in the same location with a certain delay τ that determines the time position of the hump. Such a signature behavior is found in all the measured pores (additional examples in Fig. S2) with an average timing of 7.5 ± 2.2 ms ($N = 25$ cells, Table 1). This recalls the molecular model of Nup153 activity (2), described as the result of the controlled collapse and release of its C-terminal FG-rich domain. However, the ACF cannot provide the directionality of the motion, but only the characteristic time of the overall collapse-release cycle. To separate the putative collapsing and releasing components of Nup153 movement we use the pair correlation function (pCF) analysis (22). In this analysis we perform a cross-correlation calculation of the time sequence at a pair of points along the orbit. At the distance of 32 pixels along the orbit, the pCF algorithm detects a sharp distribution of Nup153-GFP transit times in both the nucleus-to-cytoplasm and cytoplasm-to-nucleus directions (Fig. 1*F*). As a negative control, almost no correlation is detected at the same distance but perpendicular to the NPC channel (Fig. 1*F* and Fig. S3). The pCF analysis reveals that the directional movement of Nup153-GFP from cytoplasm to nucleus (3.0 ± 0.7 ms, $N = 25$; Table 1) is slightly faster compared to the one from nucleus to cytoplasm (5.1 ± 0.9 ms; Table 1) (see also Fig. S4). These data are compatible with the idea that Nup153-GFP acts as a molecular spring alternating a fast collapse into compact molecular conformations and a slightly slower release into extended conformations. Remarkably, atomic force microscope measurements showed similar properties of Nup153 in an in vitro reconstituted transport assay (14). In the same report, the authors show by immunogold electron microscopy how the FG-carboxy-terminal domain of Nup153 (here tagged to GFP) topologically maps two positions separated by approximately 100 nm within the NPC, corresponding to its extended and collapsed conformations (14), in good agreement with our findings.

Kapβ1-GFP Directed Motion Through the NPC. If the Nup153-GFP dynamics highlighted above truly reflect functional pore activity, then Nup153 vectorial motion should correlate with the motion of the molecules transported by the same mechanism. We recently showed that, similarly to Nup153, the transport of the classical Kapβ1 receptor at the NPC is regulated so as to produce a peculiar hump in the ACF (16) (Table 1). Here we report results from a two-color data acquisition on cotransfected Kapβ1-GFP and mCherry (Fig. 2 *A* and *B*) in which we concomitantly measure active and passive fluxes at the NPC. The pCF analysis demonstrates that Kapβ1 movement through the NPC must be directed, as it is univocally described by a single time of transport from cytoplasm to nucleus (Fig. 2 *C* and *D*) and from nucleus to cytoplasm (Fig. 2 *E* and *F*). Untagged mCherry yields instead a broad distribution of transit times in both directions (Fig. 2 *C–F*) (i.e., passive diffusion is not able to order molecules in time and space). As a further control, the pair cross-correlation function (pcCF) was calculated to look for any possible coupling between translocating Kapβ1 and mCherry molecules. As expected no (pair cross) correlation was detected in both the cytoplasm-to-nucleus (Fig. 2*C*, *Right carpet* ; Fig. 2*D*, blue curve) and nucleus-to-cytoplasm direction (Fig. 2*E*, *Right carpet*; Fig. 2*F*, blue curve). The individual average transit times for active and passive transport (Table 1) are in agreement with reported values (23–25) and with the pCF-based estimate obtained by sampling over several microns across the nuclear envelope (26). It is worth noting that, contrary to Nup153, Kapβ1 shows a highly symmetric pCF profile in the two directions of transport (Table 1). In light of what was observed so far, this result suggests that Kapβ1 may be affected by two independent, although similar, mechanisms: one operating from cytoplasm to nucleus [possibly mediated by Nup153, (14)] and the other from nucleus to cytoplasm (yet to be identified).

Nup153-Mediated Cargo Transport Across the NPC. To probe the involvement of Nup153 in promoting molecular translocations from cytoplasm to nucleus, we performed an experiment in which Nup153-GFP is coexpressed with a mCherry-tagged nuclear localization sequence (NLS) (Fig. 3*A*). NLS-mCherry is actively transported into the nucleus by a Kapβ1-driven process while it moves back to the cytoplasm by passive diffusion (27) (Fig. 3*B*). Under these conditions Nup153-GFP behaves as expected in terms of ACF profile (Fig. 3*C*), cytoplasm-to-nucleus "collapse" (Fig. 3*D*, *Left carpet*; Fig. 3*E*, green curve), and nucleus-to-cytoplasm "release" (Fig. 3*F*, *Left carpet*; Fig. 3*G*, green curve). Concomitantly, NLS-mCherry yields two characteristic distributions of transit times (active + passive) from cytoplasm to nucleus (Fig. 3*D*, *Middle carpet* ; Fig. 3*E*, red curve), but only one (passive) from nucleus to cytoplasm (Fig. 3*F*, *Middle carpet*; Fig. 3*G*, red curve). Remarkably, by pCF we show that NLS-mCherry motion is correlated in time and space with that of Nup153-GFP along the cytoplasm-to-nucleus direction of the NPC (Fig. 3*D*, *Right*

*In the tracking experiment the PSF is scanned around the distribution of fluorescence of the analyzed protein. Depending on the protein this distribution may not coincide to the real center of mass of the entire NPC (to which we refer for simplicity).

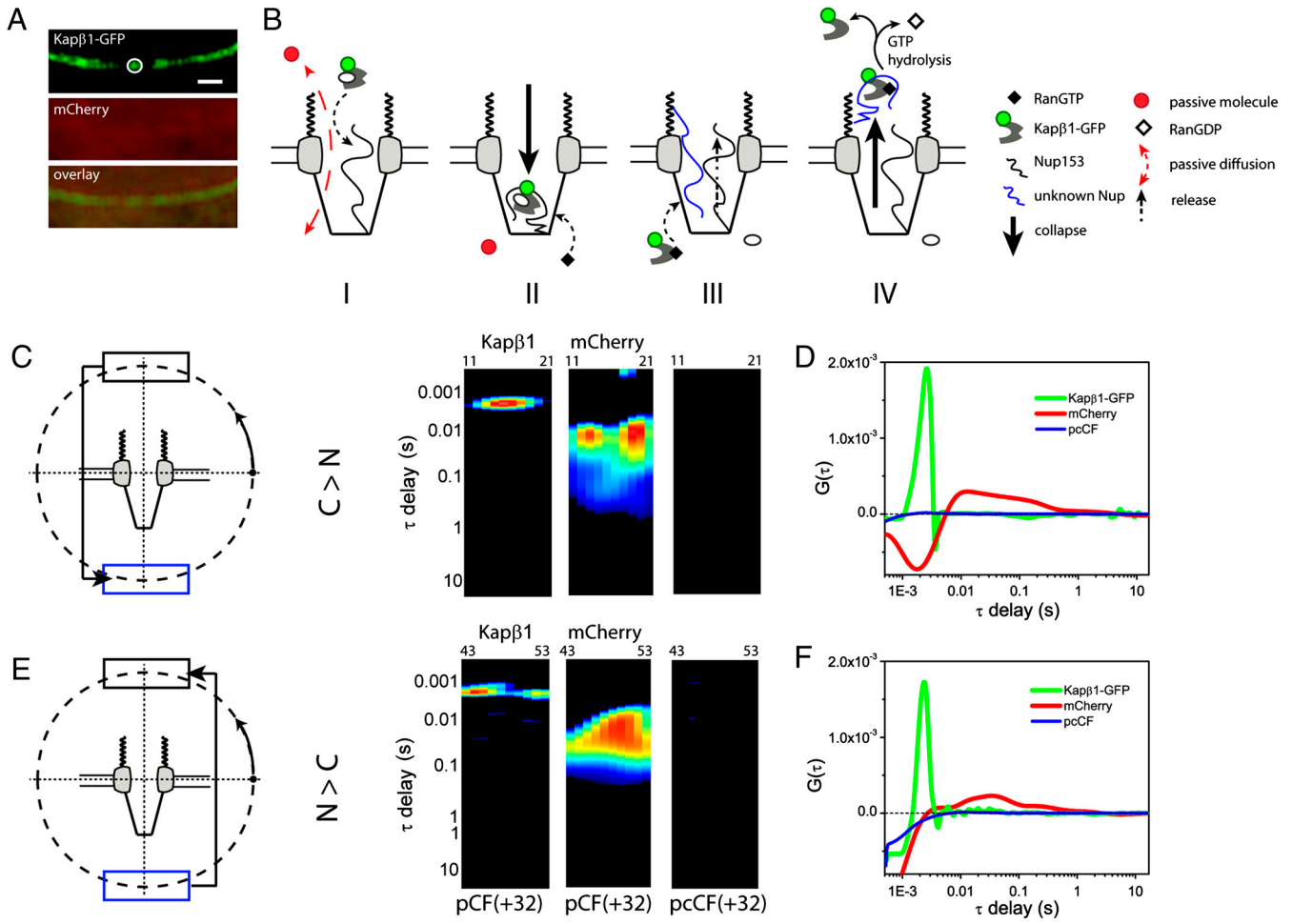

Fig. 2. (*A*) Kapβ1-GFP is cotransfected with untagged mCherry (scale bar: 1 μm). (*B*) In the schematic diagram, an unlabeled Nup153 (the endogenous one, in this experiment) mediates Kapβ1-GFP movement towards the nucleus (I and II); a symmetric process must exist to account for Kapβ1 movement towards the cytoplasm (III and IV). The mCherry molecule passively diffuses back and forth with no interaction with Nup153. (*C* and *D*) The pCF(+32) from cytoplasm to nucleus shows a sharp distribution of Kapβ1 transolaction times (*Left carpet*, green curve) opposed to a much broader distribution of mCherry translocation times (*Middle carpet*, red curve). The pcCF(+32) shows that Kapβ1-GFP and mCherry are not translocating together from cytoplasm to nucleus (*Right carpet*, blue curve). (*E* and *F*) The pCF and pcCF at the distance of 32 pixels from nucleus to cytoplasm reveal the symmetry of the observed behaviors: Kapβ1 rapidly translocates, independently from mCherry passive diffusion.

carpet; Fig. 3*E*, blue curve). The positive pair-cross-correlation signal suggests that at least a subpopulation of NLS-mCherry molecules may be effectively exploiting Nup153-GFP to move from cytoplasm to nucleus across the NPC. A relevant control for this conclusion is that no pcCF signal can be observed in the opposite direction (Fig. 3*F*, *Right carpet* ; Fig. 3*G*, blue curve), where NLS-mCherry passive diffusion is not coupled to Nup153-GFP dynamics.

Conclusions

An accurate picture of how selective gating is achieved by the FG-Nups remains unclear due to a general lack of understanding with regard to their behavior within the NPC. The source of this ambiguity stems in part from the difficulty in addressing FG-Nups dynamics in the intact NPC. The thought-provoking idea here is that we can overcome these limitations by a combination of tracking and fluctuation analysis to study the behavior of single pore components with high spatial and temporal resolution in live, minimally perturbed cells. The crucial point in our results is the observation of a previously hidden dynamics of nucleoporin Nup153, characterized by a rapid, discrete exchange between two separate positions within the NPC of intact cells. The nanomechanical mechanism suggested by our results highlights apparent differences with some macroscopic views proposed thus far that deserve consideration. The bulk-like hydrogel meshwork model (5), for instance, places a greater importance on the hydrophobic interactions between neighbor FG-Nups, as they are able to form a sieve-like meshwork in vitro (10). Transport could then occur through binding of transport receptors to FG-repeats, causing a local gel-to-liquid transition and allowing the receptor to catalyze its own diffusion (28). Our data do not exclude that these interactions play a role in transport; however, they suggest that the most kinetically relevant events in the intact NPC have the characteristics of directed transport, not of unbiased diffusion. It must be noted that Nup153 belongs to the FxFG-rich family of nucleoporins, which generally display noncohesive properties (29). At the same time, however, it was recently reported that C-terminal fragments of Nup153 can exist in a collapsed state but are concomitantly able to form a hydrogel in vitro (30). Besides highlighting the multifaceted character of Nup153, these contrasting results may also reflect a more general complexity of the NPC function, with a not yet completely understood balance/interplay between cohesive (i.e., gel-like) and noncohesive (i.e., "spring-like") properties, as also emerges from the hybrid model recently proposed by Yamada and coworkers (15). Based on our results on intact cells, we propose that molecular transport through the NPC can be powered, at least in part, by the directed motion of specific nucleoporins (here Nup153). Further experi-

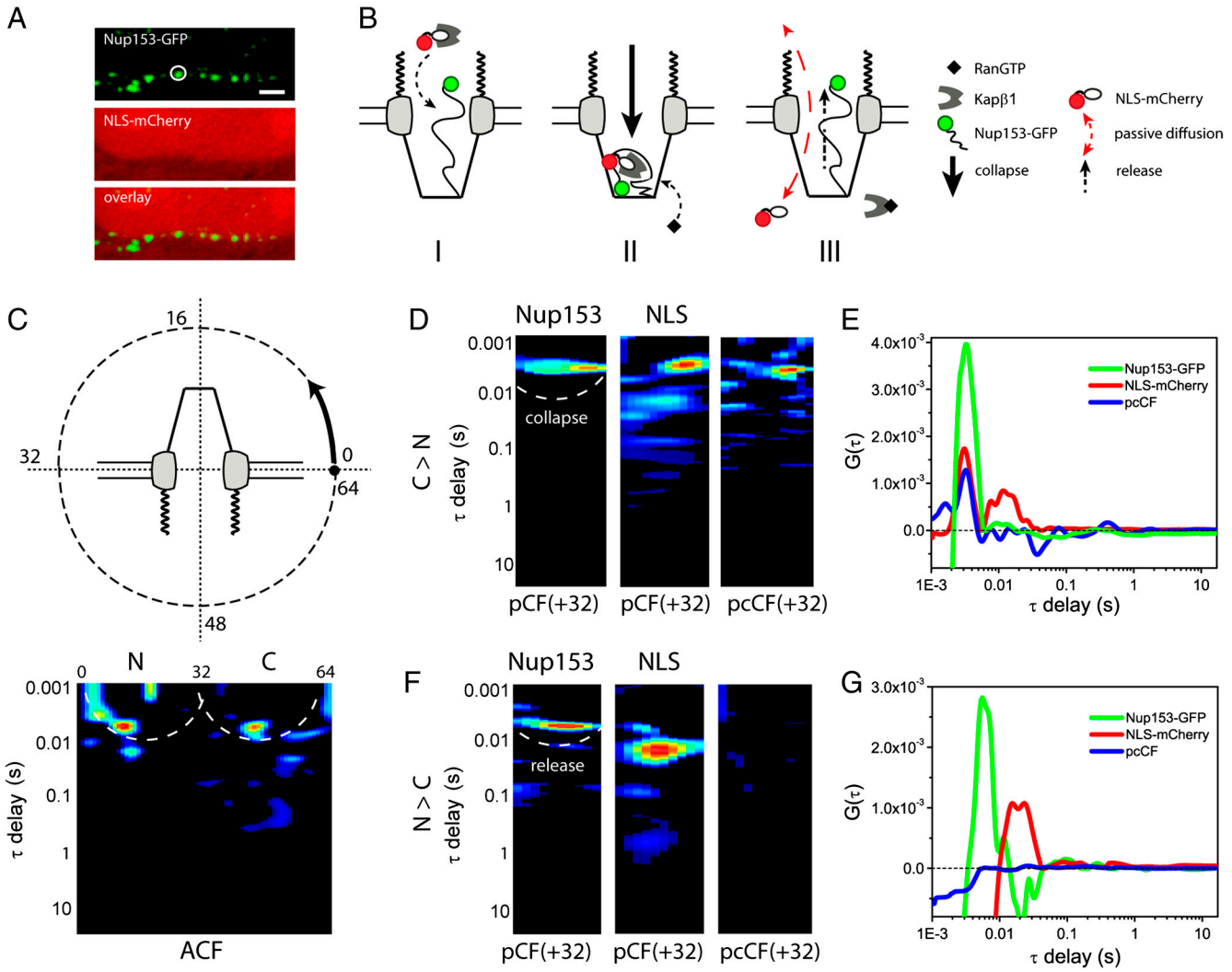

Fig. 3. (*A*) Nup153-GFP is cotransfected with NLS-mCherry (scale bar: 1 μm). (*B*) In the schematic diagram, Nup153-GFP drives NLS-mCherry towards the nucleus (I, II); the intervention of RanGTP detaches NLS-mCherry and releases Nup153-GFP (III). (*C*) The ACF yields the double-arc, characteristic of Nup153 activity at the NPC. (*D* and *E*) The pCF(+32) analysis in the cytoplasm-to-nucleus direction yields the expected distribution of Nup153 collapse times (*Left carpet*, green curve); NLS-mCherry instead shows a bimodal distribution of transit times, in keeping with the presence of two translocation mechanism (active + passive). Only the faster component (active) pair cross-correlates with Nup153 movement in this direction (*Right carpet*, blue curve). (*F* and *G*) The pCF(+32) in the opposite direction shows the expected distribution of Nup153 release times (*Left carpet*, green curve) opposed to a broader distribution of NLS-mCherry passive translocation times (*Middle carpet*, red curve). The pcCF(+32) analysis shows that Nup153-GFP and NLS-mCherry are not moving bound together in this direction, as expected (*Right carpet*, blue curve).

ments on additional constituents of the pore (e.g., more cohesive Nups of the central channel) are needed to achieve more general conclusions about the intimate nature of selective molecular gating through the NPC. Finally, it is worth noting that the observed directed-motion mechanism shares many biochemical and physical characteristics with several spring-like molecular systems present in nature (31). We shall argue that they represent ancient and commonplace eukaryotic molecular engines.

Materials and Methods

Cell Culture, Plasmids, and Treatments. CHO-K1 cells were grown in Ham's F12K medium supplemented with 10% of fetal bovine serum at 37 °C and in 5% CO_2. Freshly split cells were plated on imaging dishes and transiently transfected using Lipofectamine 2000 according to manufacturer's protocol, 24 h before the experiment. The plasmid encoding for Nup153-GFP was a kind gift from Nathalie Daigle (Cell Biology and Biophysics Unit, European Molecular Biology Laboratory, Heidelberg, Germany) (20). The plasmid encoding for human Kapβ1-GFP was a generous gift from Marilena Ciciarello (Istituto di Biologia e Patologia Molecolari, Consiglio Nazionale delle Ricerche) (32). The plasmid encoding for NLS-mCherry has been described in a previous publication (27).

Single NPC Tracking Setup. Tracking of single NPCs was performed using a home-built microscope capable of single particle tracking, whose details have been already described (33). Briefly, the microscope is built around an Olympus X71 body. A Chameleon Ultra (tunable) Ti:Sapphire laser (Coherent) tuned at 940 nm was used for two-photon excitation of the GFP (and mCherry) constructs. The scanning of the excitation light was obtained in the *x–y* plane and in the *z* axis through two galvano-motor driven mirrors (Cambridge Technology) and a piezo-objective positioner (Phisik Instrument) respectively, both driven by a computer card (three-axis card, ISS). Fluorescence emission was collected by a 1.2-NA water objective (Olympus UplanSApo 60x), split by a dichroic mirror at 570 nm and detected in the 500–550 nm (GFP) and 575–645 nm (mCherry) spectral ranges by two GaAS detectors H7241P (Hamamatsu). During the tracking procedure, the two scanning mirrors are moved independently by $\pi/2$-phase shifted sine wave voltages generated in the card so that the laser beam moves in a circular path around the particle. The position of the scanning center is determined by the offset values of the sine waves. The position of the center is updated at each tracking cycle according to the fast Fourier transform (FFT)-based algorithm previously described (34). From the FFT of the intensity trace along the orbit, we get the average intensity or dc as the zeroth term in a Fourier series and the ac as the coefficient of the first harmonic term. The angular coordinate of the particle is given directly by the phase of the ac term, and its distance from the center

can be calculated from the modulation of the signal, defined as mod = ac/dc, so that its position can be recovered. The tracking routine changes the coordinates of the center of the scanning orbit in such a way to keep the modulation at a minimum, i.e., to keep the particle always at the center. The tracking procedure started by acquiring a raster scan image of the sample, focusing on the equatorial section of the nuclear envelope. Then we clicked on a location on the image corresponding to an isolated NPC. The fluorescence intensity is collected at 64 points along a circular orbit around the pore, with a period of 0.5–1 ms and a calibrated scanning start point. The orbit radius (R) is usually set to 120 nm, which we found to be optimal for the tracking. The optimal radius for tracking a point-like particle should be on the order of half the size of the PSF (34), but in our case this value is slightly larger due to the finite size of the NPC. The position of the center of the scanning orbit is updated typically every 32–64 orbits (that is defined as the cycle), which is fast enough to follow the NPC movement. The acquisition time for a single NPC tracking measurement typically varied from 15 s up to 100 s. For each NPC we acquired the intensity along the orbit for one or two channels and the trajectory of the center of mass. From the recorded trace of the fluorescence intensity along the orbit the value of the modulation of the signal can be calculated at each cycle. The analysis of the modulation allows to check a posteriori if the particle has been tracked correctly for the entire acquisition or to exclude the portions of the dataset where the particle was temporarily or definitely lost. We selected only the part of the data acquired with the orbit centered and stationary with respect to the center of mass of the NPC.

Fluctuation Analysis. The fluctuation analysis of the data was performed with the SimFCS software (www.lfd.uci.edu, University of California at Irvine) using the scanning-FCS analysis tool, as thoroughly described in previous publications (22, 26). Briefly, the ACF, pCF(pixels), and pcCF(pixels) are displayed in pseudo colors in a carpet in which the *x* coordinate corresponds to the point along the orbit and the vertical coordinate corresponds to the correlation time in a log-scale.

ACKNOWLEDGMENTS. We thank Milka Stakic for helping in cultivating and transfecting the CHO-K1 cells. This work was supported by the National Center for Research Resources (5P41RR003155), the National Institute of General Medical Sciences (8P41GM103540), divisions of the National Institutes of Health (NIH), and NIH 5P50 GM076516.

1. Weis K (2003) Regulating access to the genome: Nucleocytoplasmic transport throughout the cell cycle. *Cell* 112:441–451.
2. Fahrenkrog B, Aebi U (2003) The nuclear pore complex: Nucleocytoplasmic transport and beyond. *Nat Rev Mol Cell Biol* 4:757–66.
3. Rout M-P, Aitchison J-D (2001) The nuclear pore complex as a transport machine. *J Biol Chem* 276:16593–16596.
4. Denning D-P, Patel S-S, Uversky V, Fink A-L, Rexach M (2003) Disorder in the nuclear pore complex: The FG repeat regions of nucleoporins are natively unfolded. *Proc Natl Acad Sci USA* 100:2450–2455.
5. Ribbeck K, Gorlich D (2002) The permeability barrier of nuclear pore complexes appears to operate via hydrophobic exclusion. *EMBO J* 21:2664–2671.
6. Conti E, Muller C-W, Stewart M (2006) Karyopherin flexibility in nucleocytoplasmic transport. *Curr Opin Struct Biol* 16:237–244.
7. Rout M-P, et al. (2000) The yeast nuclear pore complex: Composition, architecture, and transport mechanism. *J Cell Biol* 148:635–651.
8. Ben-Efraim I, Gerace L (2001) Gradient of increasing affinity of importin beta for nucleoporins along the pathway of nuclear import. *J Cell Biol* 152:411–417.
9. Peters R (2005) Translocation through the nuclear pore complex: Selectivity and speed by reduction-of-dimensionality. *Traffic* 6:421–427.
10. Frey S, Richter R-P, Gorlich D (2006) FG-rich repeats of nuclear pore proteins form a three-dimensional meshwork with hydrogel-like properties. *Science* 314:815–817.
11. Frey S, Gorlich D (2009) FG/FxFG as well as GLFG repeats form a selective permeability barrier with self-healing properties. *EMBO J* 28:2554–2567.
12. Frey S, Gorlich D (2007) A saturated FG-repeat hydrogel can reproduce the permeability properties of nuclear pore complexes. *Cell* 130:512–523.
13. Lim R-Y, et al. (2006) Flexible phenylalanine-glycine nucleoporins as entropic barriers to nucleocytoplasmic transport. *Proc Natl Acad Sci USA* 103:9512–9517.
14. Lim R-Y, et al. (2007) Nanomechanical basis of selective gating by the nuclear pore complex. *Science* 318:640–643.
15. Yamada J, et al. (2010) A bimodal distribution of two distinct categories of intrinsically disordered structures with separate functions in FG nucleoporins. *Mol Cell Proteomics* 9:2205–2224.
16. Cardarelli F, Lanzano L, Gratton E (2011) Nanoscale fluorescence correlation spectroscopy of intact nuclear pore complexes. *Biophys J* 101:L27–29.
17. Ball J-R, Ullman K-S (2005) Versatility at the nuclear pore complex: Lessons learned from the nucleoporin Nup153. *Chromosoma* 114:319–330.
18. Fahrenkrog B, et al. (2002) Domain-specific antibodies reveal multiple-site topology of Nup153 within the nuclear pore complex. *J Struct Biol* 140:254–267.
19. Rabut G, Doye V, Ellenberg J (2004) Mapping the dynamic organization of the nuclear pore complex inside single living cells. *Nat Cell Biol* 6:1114–1121.
20. Daigle N, et al. (2001) Nuclear pore complexes form immobile networks and have a very low turnover in live mammalian cells. *J Cell Biol* 154:71–84.
21. Pante N, Thomas F, Aebi U, Burke B, Bastos R (2000) Recombinant Nup153 incorporates in vivo into Xenopus oocyte nuclear pore complexes. *J Struct Biol* 129:306–312.
22. Digman M-A, Gratton E (2009) Imaging barriers to diffusion by pair correlation functions. *Biophys J* 97:665–673.
23. Yang W, Gelles J, Musser S-M (2004) Imaging of single-molecule translocation through nuclear pore complexes. *Proc Natl Acad Sci USA* 101:12887–12892.
24. Kubitscheck U, et al. (2005) Nuclear transport of single molecules: Dwell times at the nuclear pore complex. *J Cell Biol* 168:233–243.
25. Dange T, Grunwald D, Grunwald A, Peters R, Kubitscheck U (2008) Autonomy and robustness of translocation through the nuclear pore complex: A single-molecule study. *J Cell Biol* 183:77–86.
26. Cardarelli F, Gratton E (2010) In vivo imaging of single-molecule translocation through nuclear pore complexes by pair correlation functions. *PLoS One* 5:e10475.
27. Cardarelli F, Bizzarri R, Serresi M, Albertazzi L, Beltram F (2009) Probing nuclear localization signal-importin alpha binding equilibria in living cells. *J Biol Chem* 284:36638–36646.
28. Eisele N-B, Frey S, Piehler J, Gorlich D, Richter R-P (2010) Ultrathin nucleoporin phenylalanine-glycine repeat films and their interaction with nuclear transport receptors. *EMBO Rep* 11:366–372.
29. Patel S-S, Belmont B-J, Sante J-M, Rexach M-F (2007) Natively unfolded nucleoporins gate protein diffusion across the nuclear pore complex. *Cell* 129:83–96.
30. Milles S, Lemke E-A (2011) Single molecule study of the intrinsically disordered FG-repeat nucleoporin 153. *Biophys J* 101:1710–1719.
31. Mahadevan L, Matsudaira P (2000) Motility powered by supramolecular springs and ratchets. *Science* 288:95–100.
32. Ciciarello M, et al. (2004) Importin beta is transported to spindle poles during mitosis and regulates Ran-dependent spindle assembly factors in mammalian cells. *J Cell Sci* 117:6511–6522.
33. Levi V, Ruan Q, Gratton E (2005) 3-D particle tracking in a two-photon microscope: Application to the study of molecular dynamics in cells. *Biophys J* 88:2919–2928.
34. Kis-Petikova K, Gratton E (2004) Distance measurement by circular scanning of the excitation beam in the two-photon microscope. *Microsc Res Tech* 63:34–49.